Applied Catalysis B: Environmental 180 (2016) 29–37

Contents lists available at ScienceDirect

Applied Catalysis B: Environmental

journal homepage: www.elsevier.com/locate/apcatb

Synthesis of oxide supported $LaMnO_3$ perovskites to enhance yields in toluene combustion

Anne Giroir-Fendler[a,*], Maira Alves-Fortunato[a], Melissandre Richard[b], Chao Wang[a,c], Jose Antonio Díaz[a], Sonia Gil[a], Chuanhui Zhang[a,c], Fabien Can[b], Nicolas Bion[b], Yanglong Guo[c]

[a] Université Lyon 1, CNRS, UMR 5256, IRCELYON, Institut de recherches sur la catalyse et l'environnement de Lyon, 2 avenue Albert Einstein, 69626 Villeurbanne Cedex, France
[b] Université de Poitiers, CNRS UMR 7285, Institut de Chimie des Milieux et Matériaux de Poitiers (IC2MP), 4 rue Michel Brunet, TSA 51106, 86073 Poitiers Cedex 9, France
[c] Key Laboratory for Advanced Materials and Research Institute of Industrial Catalysis, East China University of Science and Technology, Shanghai 200237, China

ARTICLE INFO

Article history:
Received 28 January 2015
Received in revised form 28 May 2015
Accepted 2 June 2015
Available online 4 June 2015

Keywords:
Environmental chemistry
Gas-phase reactions
Heterogeneous catalysis
Perovskite phases
Toluene oxidation
Oxygen isotopic exchange

ABSTRACT

Perovskite-type oxides of $LaMnO_3$ were synthesized by citrate sol-gel method in the presence of an oxide support. The physicochemical properties of the $LaMnO_3$ supported materials were characterized by inductively coupled plasma atomic emission spectroscopy (ICP-AES), thermogravimetric and differential thermal analysis (TGA/DTA), N_2 adsorption–desorption, X-ray diffraction (XRD), high transmission electron microscopy (HRTEM-EDX) and oxygen isotopic exchange analysis. Their catalytic performances, especially those related to the catalyst stability, were evaluated for the total oxidation of toluene. To this aim, three consecutive catalytic cycles were performed for each catalyst. The $LaMnO_3$ perovskite phase appeared to interact with TiO_2 and Y_2O_3–ZrO_2 (YSZ) supports in a manner that affected both oxygen mobility and catalytic activity in total toluene oxidation. The isotopic exchange results matched well the catalytic tests. Indeed, the supported materials showed a remarkable oxygen exchange activity and higher catalytic performances than that of pure perovskite. For YSZ, this could be attributed to the influence of oxygen vacancies and oxygen ions on the support. Regarding TiO_2, this improvement could be attributed to the reducibility properties of titania (Ti^{IV}/Ti^{III}). Strong metal-support interactions (SMSI) between the perovskite and the support were observed.

1. Introduction

Noble metal-based catalysts (containing platinum, palladium, and rhodium) are currently preferred for the catalytic pollution control of exhaust gases emanating from the combustion process. These noble metals, even at low metal loadings and low temperature, are very effective for catalytic combustion, but the steady increase of noble metal prices represents a critical disadvantage. In addition, such catalysts tend to sinter and deactivate through the production of Cl and sulfur compounds. Given this context and the constant reinforcement of government regulations concerning CO, NO_x, SO_x, HC, soot, and VOC emissions [1], the development of alternative catalytic technologies and materials has been promoted. Perovskite-type oxides have been studied as a low-cost material substitute for noble metals in electrocatalysis [2], in catalytic oxidation for hydrocarbons and VOCs [3] and in SCR for NO_x removal [4–9] since the early 1970s. They have been proven to be very efficient for catalytic combustion at low temperatures ($\leq$400 °C) and present high thermal stability ($\geq$1000 °C) compared to noble metals. These oxides have a well-defined crystalline structure generally represented as ABO_3. Cation A is of larger ionic radius – generally a rare earth element, an alkaline earth metal or an alkali metal – while cation B is of smaller ionic radius, generally a transition metal from the 3d, 4d or 5d group [10,11].

Practical applications of perovskites in catalytic combustion are nonetheless currently limited due to their very low specific surface area (SSA), < ~20 $m^2\,g^{-1}$, which limits their value for use in onboard catalytic processes. The preparation of high SSA perovskites is therefore important for the future application of these materials in catalytic combustion reactions. Several meth-

* Corresponding author. fax: +33 472431695.
E-mail address: anne.giroir-fendler@ircelyon.univ-lyon1.fr (A. Giroir-Fendler).

http://dx.doi.org/10.1016/j.apcatb.2015.06.005
0926-3373/

ods have been employed in order to produce perovskites with high SSA (<100 $m^2 g^{-1}$), such as co-precipitation [12], solid–solid [13] or solid-gas routes [14], nanocasting [15], freeze-drying [16], and mechano-synthesis at low calcination temperature [17]. These methods, however, generally require several steps and complex routes for good results.

The aim of this work was to develop supported $LaMnO_3$ perovskite over different oxides supports: Y_2O_3–ZrO_2 (YSZ, ionic conductor) and TiO_2 (electronic conductor), to increase the accessible surface of perovskite material. Then, their catalytic performances were evaluated for the catalytic oxidation of toluene (model reaction). The attention was focused on the catalyst stability during three consecutive cycles. The long-term toluene oxidation test, running for 24 h at 50% of toluene conversion, was also carried out. Moreover, the oxygen isotopic exchange technique, a well known technique for reactions of oxygen isotopes with metal oxide supported systems, was used to better understand the behavior of the catalytic systems [18–22].

2. Experimental

2.1. Catalyst preparation

2.1.1. Preparation of $LaMnO_3$

The citrate route was used to prepare $LaMnO_3$ perovskites (denoted LM). First, $La(NO_3)_3.6H_2O$ (Sigma–Aldrich, >99.0%), $Mn(NO_3)_3.4H_2O$ (Alfa Aesar, 98%), and citric acid anhydrous (Alfa Aesar, >99.5%) were diluted in 25 mL deionized water. The solution was maintained at 90 °C for 2 h under stirring (600 rpm), followed by drying for one night at 110 °C. After that, the resulting sample was milled and submitted to a static thermal treatment in an oven at 1 °C min^{-1} up to 200 °C in order to eliminate the citric acid. The calcination of the sample was then performed under 50 mL min^{-1} air flow at 750 °C for 2 h at a ramp temperature of 5 °C min^{-1}.

2.1.2. Preparation of supported perovskites

The citrate route was also used to prepare supported perovskites, where the precursors were the same as those used for $LaMnO_3$ preparation. Thus, $La(NO_3)_3.6H_2O$, $Mn(NO_3)_3.4H_2O$, and citric acid anhydrous were diluted in 25 mL deionized water. The solution was maintained at 90 °C for 30 min under stirring (600 rpm), and after that the calcined oxide support was slowly introduced into the stirring solution in the necessary amount to obtain 15 wt.% $LaMnO_3$. The solution was then maintained at 90 °C for 2 h under stirring, followed by drying for one night at 110 °C. Finally, the resulting sample (supported perovskite) was milled and submitted to a static thermal treatment in an oven at 1 °C min^{-1} up to 200 °C in order to eliminate the citric acid. After that, the calcination of the supported perovskite was performed under 50 mL min^{-1} air flow at 750 °C for 2 h at a ramp temperature of 5 °C min^{-1}.

The oxide supports used were: TiO_2 (DT-51, Millennium Inorganic Chemicals) and YSZ (8 mol% Y_2O_3-stabilized ZrO_2, TOSOH). These commercial supports were calcined at 750 °C (the same calcination procedure used for $LaMnO_3$ alone and supported perovskites) under air for 2 h before to be used to the supported perovskites synthesis. Note: before the calcination procedure, the TiO_2 support was present in the anatase phase with a specific surface area of 80 $m^2 g^{-1}$, and the YSZ support presented a specific surface area of 14 $m^2 g^{-1}$ with cubic structure.

2.2. Catalyst characterization

Perovskite loading was measured by inductively coupled plasma atomic emission spectroscopy, ICP-AES (Varian).

N_2 adsorption–desorption at 77 K was performed on a Quantachrom, Mod. 120 Nova 2000. Before the measurement, the samples were degassed at 300 °C for 3 h. The specific surface area (SSA) of each sample was obtained by the Brunauer–Emmett–Teller (BET) method.

Catalyst morphology and micro-structure, as well as $LaMnO_3$ size and dispersion over supports, were analyzed by TEM (Transmission Electronic Microscopy, JEOL 2010 LaB6).

Powder X-ray diffraction (XRD) patterns were recorded on a Bruker D5005 diffractometer equipped with a CuKα radiation (λ = 1.5418 Å) and a graphite monochromator on the diffracted beam, and the XRD datas were generally collected in the 2θ range of 4–80° with a scanning step size of 0.02° and 0.5 s. The mean crystallite size (d_s) of supports, the perovskite and the supported perovskites were calculated from the line broadening of the most intense reflections using the Scherrer equation:

$$d_s = \frac{k \times \lambda}{\beta \times \cos(\vartheta)} \quad (1)$$

where d_s is the mean size of the ordered (crystalline) domains, k (0.9) is the shape factor, λ (1.54 Å) is the x-ray wavelength, β is the line broadening at half the maximum intensity (FWHM) in radians, and θ is the Bragg angle.

Thermogravimetric and differential thermal analysis, TGA/DTA (SETARAM, Setsys Evolution 12), were carried out with 5–10 mg of sample, under air flow, from 25 °C to 900 °C, using the same temperature ramp (5 °C min^{-1}) than the heating ramp used during material preparation (calcinations procedure).

H_2-TPR measurements were conducted on a self-designed setup equipped with a U-shaped quartz reactor and an INFICON IPC400 quadrupole mass spectrometer (MS). After cooling down to room temperature, 30 mL min^{-1} of 5 vol.% H_2/He mixture gas was introduced until stabilization of MS baseline. Then the reactor was heated at a ramp of 15 °C min^{-1} from room temperature to 900 °C. Simultaneously, the signal of consumed H_2 at m/e = 2 was recorded by the MS detector.

2.3. Catalyst testing

The catalytic test was carried out with 100 mg of catalyst placed over quartz wool in a U-type reactor. The reactive mixture containing 1000 ppm C_7H_8, synthetic air (80/20) at 100 mL min^{-1} was introduced at room temperature followed by an initial temperature ramp of 5 °C min^{-1} up to 80 °C for 30 min to stabilize the signal, followed by a second temperature ramp of 2 °C min^{-1} up to 450 °C. After this treatment, all catalysts were tested during the cooling ramp. This sequence was repeated three times. During the consecutive runs reproducible results were obtained for toluene oxidation. Moreover, the catalytic stabilization was also evaluated with a long-term toluene oxidation test, running for 24 h at 50% of toluene conversion for all catalysts. The total conversion of toluene (X) was defined as follows:

$$X_{C_7H_8}(\%) = 100 \times \frac{[C_7H_8]_{in} - [C_7H_8]_{out}}{[C_7H_8]_{in}} \quad (2)$$

where $[C_7H_8]_{in}$ and $[C_7H_8]_{out}$ denoted the inlet and outlet concentrations of toluene, respectively.

2.4. Analysis of products

Toluene and possible organic products were analyzed by gas chromatography (CPG, PERKIN ELMER Clarus 500) equipped with a flame ionization detector (FID) and TCD, using a capillary column (Chromosorb 101) for organic gas separation and a packing column (Carboxen 1000) for permanent gas separation. In addition, CO and CO_2 were continuously measured on-line by IR analyzer (ROSE-

Table 1
Physicochemical properties of supports and supported $LaMnO_3$, after calcination at 750 °C.

	Calcined TiO_2 (fresh TiO_2)	Calcined YSZ (fresh YSZ)	LM	LM/TiO_2	LM/YSZ
BET surface area (m^2g^{-1})	40 (80)	13 (14)	8	33.6	13
Total pore volume ($cm^3\ g^{-1}$)	0.12 (0.27)	0.05 (0.06)	0.05	0.16	0.08
Mean pore diameter (nm)	16.9 (11.5)	13.8 (14.9)	19.7	17.5	19.3
BET surface area ATO[a] (m^2g^{-1})	38	13	8	33	12
La:Mn ratio (mol/mol)[b]	–	–	0.97	1	1.1
wt.% perovskite	–	–	13.6	13.5	13.5
Support phase (XRD)	Rutile (Anatase)	Cubic (Cubic)	–	Rutile	Cubic
d_{LM} (nm) (XRD)	–	–	17.6	21.2	14.5
d_{TiO2} (nm) (XRD)	23.3	–	–	22.6	–
d_{YSZ} (nm) (XRD)	–	18.2	–	–	17.4

[a] After toluene oxidation (ATO).
[b] Actual La:Mn ratio loading determined by ICP analysis.

MOUNT Xstream). No other organic hydrocarbons were detected in the products.

2.5. Oxygen isotopic exchange

The oxygen isotopic exchange experiments were performed in a closed setup already described elsewhere [23,24]. A U-form reactor was placed in a closed recycle system which was connected on one side to a mass spectrometer (Pfeiffer Vacuum, QMS 200) for the monitoring of the gas phase composition, and on the other side to a vacuum pump. A recycling pump placed in the system removed limitations due to gas-phase diffusion. Temperature programmed and isothermal oxygen isotopic exchange (TPOIE and IOIE respectively) experiments were performed with 20 mg of catalysts. Samples were pretreated under pure $^{16}O_2$ flow at 700 °C during 1 h prior to cooling down to either 200 °C for TPOIE or to 450 °C for IOIE, and thereafter evacuated during 30 min. A 55 mbar dose of pure $^{18}O_2$ (Isotec, 99.9%) was then introduced in the system and the heterolytic exchange reaction started ($^{18}O_{2(g)} + {}^{16}O_{(s)} \rightarrow$ à $^{18}O^{16}O_{(g)} + {}^{18}O_{(s)}$ *simple exchange*). For TPOIE experiments, the temperature was increased from 200 °C to 700 °C with a ramp rate of 2 °C/min. Temporal evolution of the concentrations of $^{18}O_2$, $^{18}O^{16}O$, $^{16}O_2$ isotopomers was continuously followed by collecting every 3 s the 36, 34, and 32 m/z values, respectively. The 28 m/z value was also monitored to detect any possible leak in the system.

The method used to follow the atomic fraction of ^{18}O in the gas-phase (α_g), to calculate the number of O atoms exchanged (N_e) and to determine the initial rate of exchange (R_e) was described elsewhere [18,23]. Typically:

$$\alpha_g = \frac{P_{36} + \frac{1}{2}P_{34}}{P_{36} + P_{34} + P_{32}} \quad (3)$$

where P_{36}, P_{34}, and P_{32} are the partial pressures of $^{18}O_2$, $^{18}O^{16}O$, and $^{16}O_2$ respectively,

$$N_e = N_g \bullet (1 - \alpha_g) \quad (4)$$

being N_g the number of ^{18}O atoms in gas-phase at the beginning of the reaction;

$$R_e = -N_g \frac{d\alpha_g}{dt} \quad (5)$$

3. Results and discussion

3.1. Catalyst characterization

The physicochemical properties of the supports, YSZ and TiO_2, and the supported $LaMnO_3$, after calcinations at 750 °C, are listed in Table 1. N_2 adsorption–desorption isotherms and pore size distributions of the calcined supports are presented in Fig. 1. Both supports presented a N_2 adsorption/desorption profile (Fig. 1a) that can be assigned to the type IV isotherm, showing a hysteresis loop due to capillary condensation representative of a mesoporous material. YSZ support presented a low specific surface area, SSA ($13\ m^2\ g^{-1}$) and pore volume ($0.05\ cm^3\ g^{-1}$), while TiO_2 support showed a high surface specific area ($40\ m^2\ g^{-1}$) and pore volume ($0.12\ cm^3\ g^{-1}$). Both supports, of mesoporous nature, had a BET surface area and pore volume in the range commonly accepted for

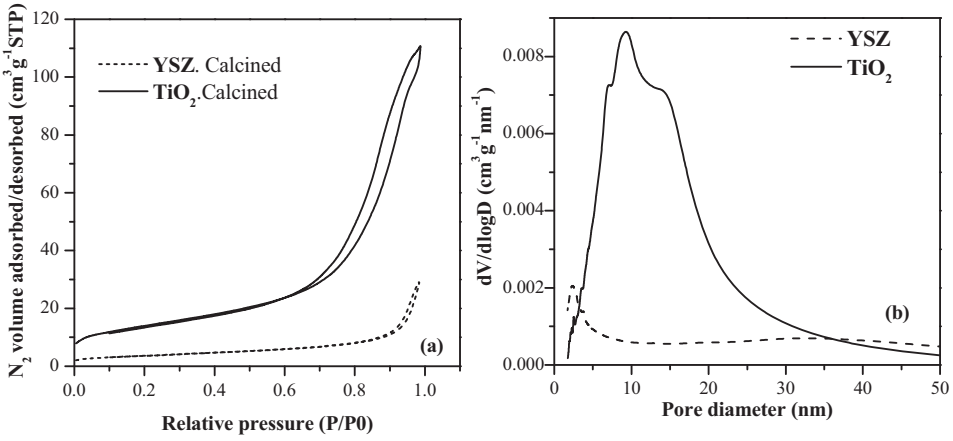

Fig. 1. (a) N_2 adsorption/desorption isotherms and (b) pore size distributions associated with calcined YSZ and TiO_2 supports.

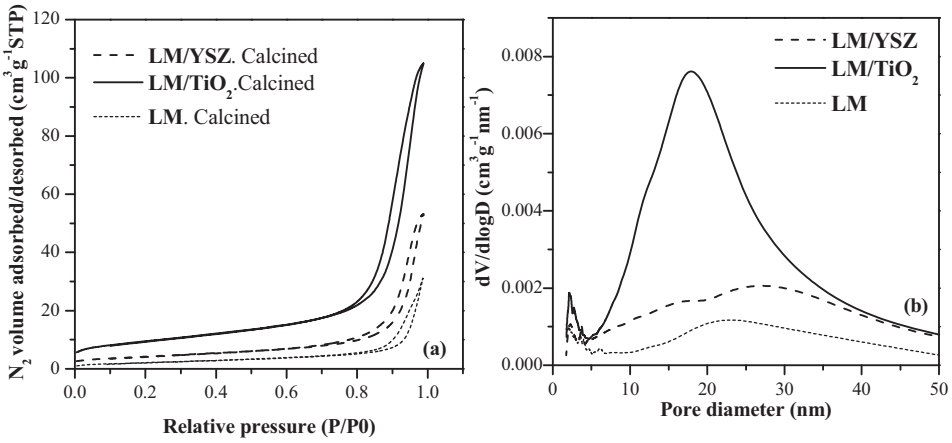

Fig. 2. (a) N_2 adsorption/desorption isotherms and (b) pore size distributions associated with perovskite alone and supported perovskites.

these materials (10–300 $m^2\ g^{-1}$). The pore size distribution (Fig. 1b) showed a double distribution in size with a predominant centered at around 2.5 nm and a second one at 35 nm for YSZ support, while the distribution of TiO_2 support showed a narrow peak centered at 9.4 nm. The supported perovskites showed a higher specific surface area and pore volume, Table 1, than pure perovskite (8 $m^2\ g^{-1}$, 0.05 $cm^3\ g^{-1}$), where the shape of the N_2 isotherms remained almost the same as those of the supports (Fig. 2). Moreover, catalyst LM/TiO_2 presented the highest specific surface area but lower than that of the TiO_2 support. This effect may be attributed to pore blockage after the perovskite incorporation. However, the catalyst LM/YSZ presented the same specific surface area the support alone. On the other hand, results listed in Table 1 showed that both the total pore volume and the mean pore diameter of the supported perovskites were greater than their respective calcined supports. This fact could be attributed to the modification of the support structure during the synthesis process, as well as to the interstice mesopore structure formed by nanoparticles assembly [25]. In addition, the thermal stability of the supports and catalysts was studied (Table 1). The specific surface of the supports and the supported perovskites decreased slightly after two and three toluene oxidation runs, respectively, which means that the properties of both supports and catalysts were not modified after the heat treatment.

The formation of the perovskite $LaMnO_3$ phase on the different supports was evaluated by XRD. XRD data of the calcined YSZ and TiO_2 supports showed the cubic fluorite structure (PDF#30-1468) and the rutile structure (JCPDS file No. 65-0190), respectively. XRD patterns of supported $LaMnO_3$ (LM) over YSZ and TiO_2 show the $LaMnO_3$ phases as well as corresponding the oxide phases (Table 1, Fig. 3a and b). The method of preparation and the further thermal treatment used seemed to be suitable for preserving the crystallographic structure of the supports while allowing the formation of the $LaMnO_3$ structure. The mean crystallite sizes (d_s) of the TiO_2 and YSZ supports were determined from XRD line broadening measurements using the Scherrer equation, where the crystallite sizes remained almost the same as those of the supports alone. Moreover, the mean crystallite size of the perovskite alone and supported perovskite was also determined, Table 1, where YSZ support promotes greater dispersion of the perovskite than the TiO_2 support.

Differential thermal analysis (DTA) shows similar profiles for all samples. Exothermic peaks were observed at low temperatures (220 °C–400 °C), which were followed by an endothermic region at 700–750 °C for catalysts LM/YSZ and LM/TiO_2, respectively (Fig. 4a). The latter endothermic region could be related to the formation of the $LaMnO_3$ structure. At lower temperatures (<220 °C), endothermic processes related to the desorption of water and nitrates were also detected (Fig. 4b). After 300 °C–400 °C, a total mass loss of 20–23% occurred for catalysts LM/TiO_2 and LM/YSZ. This loss of mass exactly corresponded, whenever the supports are considered to be stable, to the theoretical value of $LaMnO_3$ formation.

HR-TEM and corresponding FFT images (Fig. 5 and Fig. 6) also confirmed the synthesis of the $LaMnO_3$ perovskite. $LaMnO_3$ perovskite was deposited onto the support as nanoparticles of 20–30 nm diameters with an orthorhombic structure (Table 2). Based on 2D images, it could be concluded that the morphology of the perovskite particle on the LM/YSZ catalyst was highly heterogeneous. Images of catalyst LM/TiO_2 (Fig. 6) showed agglom-

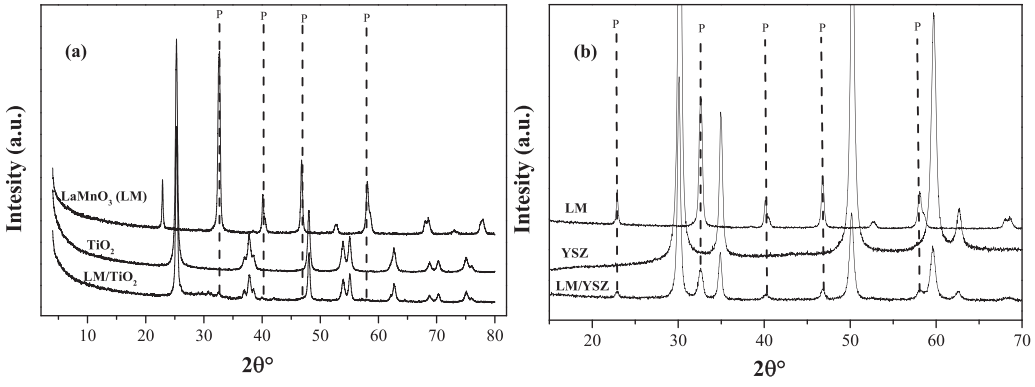

Fig. 3. XRD patterns of pure $LaMnO_3$, calcined support and supported $LaMnO_3$ on (a) TiO_2 support and (b) YSZ support. (P) corresponds to the $LaMnO_3$ phases.

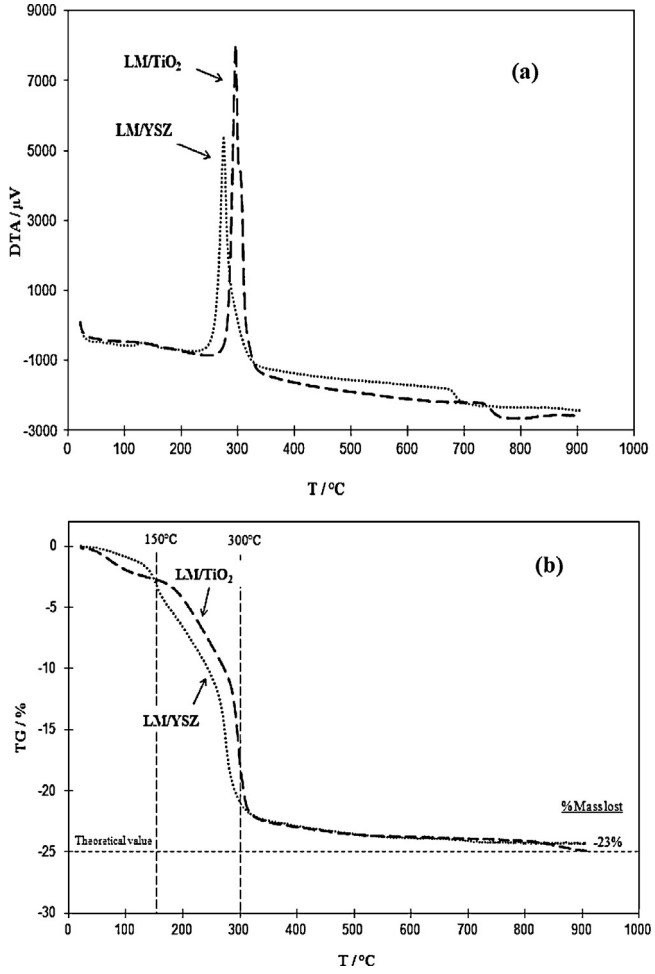

Fig. 4. DTA (a) and TGA (b) profiles obtained for catalysts LM/TiO_2 and LM/YSZ under air, using the same temperature ramp ($5\,^{\circ}C\,min^{-1}$) than the heating ramp used during material preparation (calcination procedure).

Table 2
Fast Fourier transform image analysis of HR-TEM of sample LM/YSZ (Fig. 3b), orthorhombic crystallographic structure, comparison between theoretical and experimental data.

h k l	d_{th}(Å)	A_{th}(°)	d_{exp}(Å)	A_{exp}(°)
2 0 2	2.24	0	2.23	0
3 1 0	1.75	39.4	1.77	38.4
1 1 −2	2.77	90.8	2.80	91
−2 2 −2	1.77	141.9	1.73	141.4

Table 3
Catalytic performances of the supported perovskite on the toluene oxidation during the cooling ramp.

	Catalysts	$LaMnO_3$	LM/TiO_2 (TiO_2 alone)	LM/YSZ (YSZ alone)
First run	$T_{50\%}$ (°C)[a]	349	278 (437)	237 (276)
	$T_{90\%}$ (°C)[a]	416	303	248 (289)
Second run	$T_{50\%}$ (°C)[a]	358	278 (438)	235 (272)
	$T_{90\%}$ (°C)[a]	425	303	247 (283)
Third run	$T_{50\%}$ (°C)[a]	352	278	237
	$T_{90\%}$ (°C)[a]	422	303	248

[a] Light-off temperatures at 50% and 90% of toluene conversion, respectively.

erations of poor-dispersed $LaMnO_3$ nanoparticles, as a consequence of the weak bonding between the perovskite and the support. Again, XRD analysis of catalysts LM/TiO_2 and LM/YSZ confirmed the orthorhombic structure of $LaMnO_3$ nanoparticles.

3.2. Catalytic tests: toluene oxidation

Catalytic performances of supported perovskites were evaluated in the total oxidation of toluene (model reaction). The catalyst stability was firstly evaluated by performing three consecutive catalytic runs for each catalyst. Fig. 7 displays the corresponding conversion-temperature profiles (light-off curves) of the pure $LaMnO_3$ catalyst during the heating and cooling ramps, whereas Table 3 lists the temperatures corresponding to 50% (T_{50}) and 90% (T_{90}) of toluene conversion. No appreciable deactivation was detected after three consecutive catalytic runs, because conversion curves overlapped each other within the experimental error (±5 °C). In addition, a stabilization of the catalyst after the first run was clearly observed. Bearing in mind the points above mentioned, further catalytic results were referred to the cooling ramp. Finally, it is worth to note that, although YSZ and TiO_2 showed a noticeable activity in toluene oxidation ($T_{50} \approx 280\,^{\circ}C$ and 440 °C, respectively), they were less active than their corresponding perovskite-based samples.

All catalysts were submitted to stability tests, at T_{50} (temperature at 50% conversion) for 24 h. Fig. 8 shows the evolution of the conversion with the time on stream. Conversion values between 45% and 53% were observed during the entire reaction time, confirming the stable catalytic performance.

The light-off curves of all perovskite-based catalysts and the corresponding supports were shown in Fig. 9. It is important to observe that supported perovskites catalyzed toluene oxidation at lower temperatures than the unsupported one. Moreover, their slopes were sharper, which suggested higher reaction rates. Therefore, the role of support in the reaction tested was clearly demonstrated. Regarding the results of supported perovskites (Fig. 9 and Table 3), it was observed that sample LM/YSZ was more active than LM/TiO_2. Indeed, T_{50} of the former was 41–43 °C lower than that of the latter.

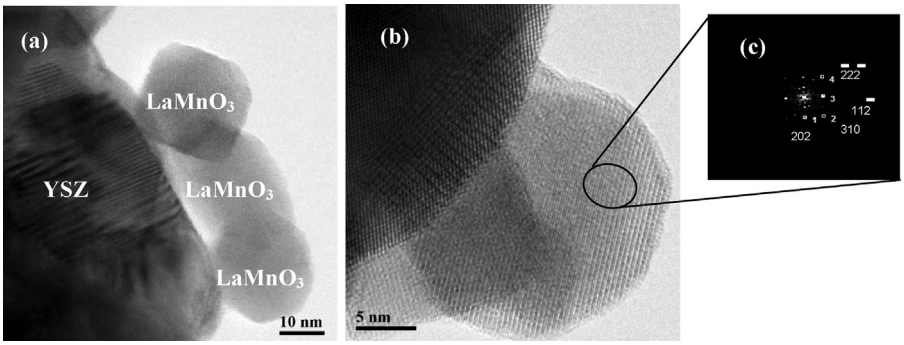

Fig. 5. HR-TEM images (a) $LaMnO_3$ nanoparticle supported on YSZ mixed oxide, (b) previous image magnification on $LaMnO_3$ orthorhombic structure, and (c) corresponding FFT image.

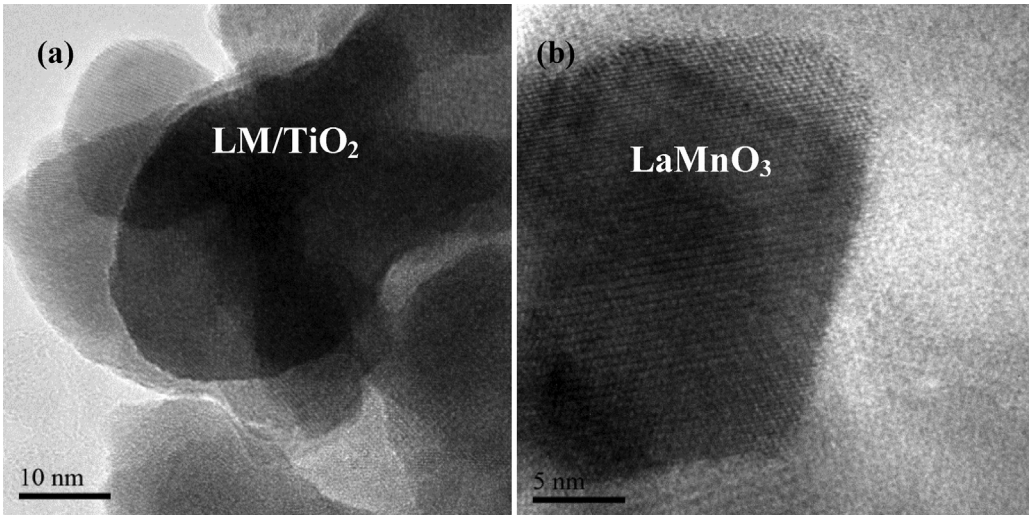

Fig. 6. HR-TEM images of (a) LM/TiO_2 and (b) magnification of LM/TiO_2.

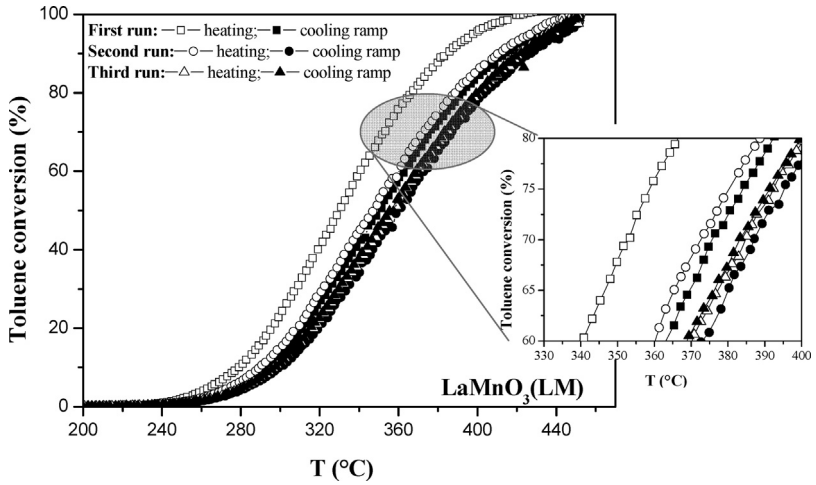

Fig. 7. Toluene conversion versus temperature during three consecutive runs (first run: -●-, second: -■-, third run: -▲-) over catalyst $LaMnO_3$ (LM), during the heating ramp (open symbol) and during the cooling ramp (full symbol).

Bearing in mind the characterization results, the better dispersion of perovskite particles over the YSZ seemed to be one of the reasons why LM/YSZ was more active than LM/TiO_2.

On the other hand, the presence of YSZ as catalytic support induced surface interactions between its oxygen vacancies and perovskite particles, which probably introduced highly reactive active sites that allowed the catalytic reaction [19]. Also, the presence of oxygen vacancies was expected to facilitate the mobility of oxygen ions from YSZ toward the surface of the support, which became highly reactive, as reported elsewhere [26,27]. Regarding the role of TiO_2, the interaction with perovskite particles seemed to be related to their reduction properties (Ti^{IV}/Ti^{III}), as already demonstrated with noble metal-supported TiO_2 [28]. Moreover, the H_2-TPR profiles of perovskite alone, TiO_2 alone and LM/TiO_2 supported perovskites are illustrated in Fig. 10. Unsupported perovskite profile showed two reduction peaks (360–430 °C), ascribed to the reduction of different species. The first peak (363 °C) could be attributed to the reduction of surface adsorbed oxygen species, as well as the reduction of Mn^{4+} into Mn^{3+}, whereas, the shoulder at about 430 °C could be related to the subsequent reduction of Mn^{3+} into Mn^{2+} [11,29,30]. On the other hand, TiO_2 alone exhibited a single reduction peak at high temperature (above 650 °C), according with results previously reported [31]. Finally, the TPR profile of LM/TiO_2 showed two peaks at 428 °C and 520 °C. The first peak could be assigned to the reduction of surface oxygen and Mn^{4+} into Mn^{3+}, whereas the second one could be attributed to not only the reduction of perovskite phase but also the reduction of TiO_2 (Ti^{4+} into Ti^{3+}). Therefore, the perovskite reduction temperature in sample LM/TiO_2 was higher than that of the perovskite alone, which revealed the interaction between both species. In addition, the reduction of TiO_2 took place at lower temperature than in the case of the support alone, which indicated that the perovskite promoted the reduction of TiO_2. Nevertheless, in order to better understand all these phenomena, isotopic exchange experiments were performed.

3.3. Oxygen isotopic exchange

TPOIE experiments were carried with samples $LaMnO_3$, TiO_2, YSZ, LM/TiO_2, and LM/YSZ. For comparative purposes, the same mass of perovskite phase was introduced into the reactor. Finally, silicon carbide (SiC) was added to obtain a total weight of the fixed bed of 20 mg.

The evolution of the ^{18}O atomic concentration was monitored in the gas phase. This way, the number of exchanged atoms in the solid (N_e) was followed with the time on stream. Fig. 11 shows, N_e as a function of temperature for each catalyst. Regarding TiO_2 sup-

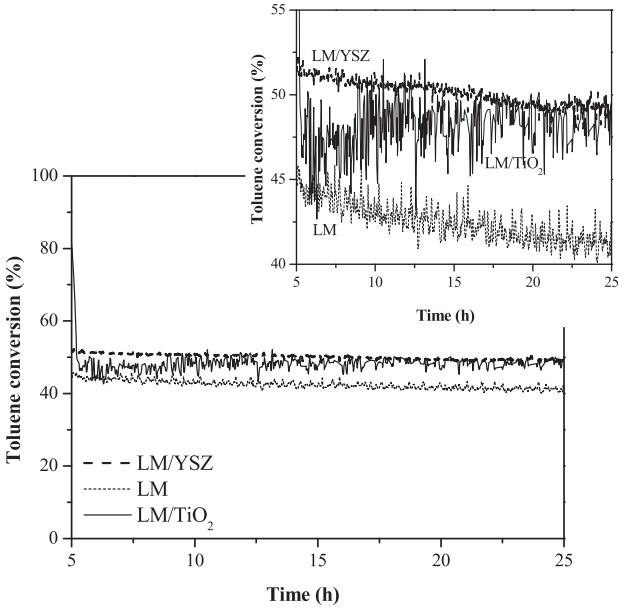

Fig. 8. The time dependence curves of toluene conversion over (dotted line) pure $LaMnO_3$, (solid line) LM/TiO_2, (dash line) LM/YSZ, running for 24 h at 50% of toluene conversion for all catalysts.

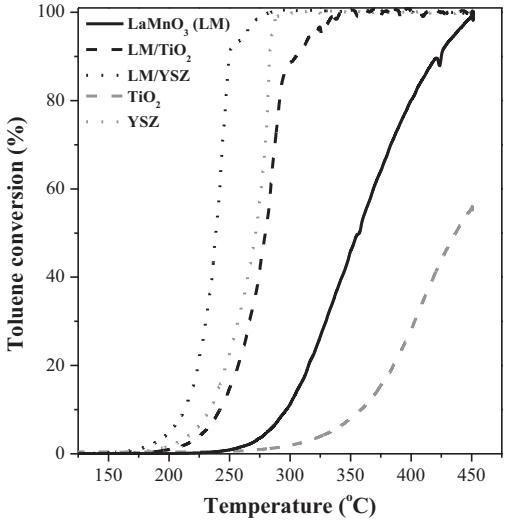

Fig. 9. The light-off curves of toluene oxidation during the third run (perovskites based catalysts) and the second run (supports) and the cooling ramp: (black solid line) pure $LaMnO_3$, (black dash line) LM/TiO_2, (black dotted line) LM/YSZ and 85% TiO_2 support (gray dash line) and 85% YSZ support (gray dotted line).

port (curve a), the oxygen exchange was almost inexistent below 675 °C. On the contrary, for the catalyst containing YSZ only (curve b), the oxygen exchange began to occur at around 475 °C, reaching high Ne values at 700 °C (40×10^{-20} at g^{-1}). This finding should be related to the oxygen ionic conductivity occurring at high temperatures [32]. The TPOIE curve of pure $LaMnO_3$ diluted with SiC (curve c) indicates that the exchange began to occur at 400 °C. Regarding the LM/YSZ catalyst (curve d), it is possible to detect an exchange activity at lower temperatures (ca 275 °C). For temperatures ranging from 250 °C to 700 °C, the number of exchanged atoms seemed to be higher in this supported solid than in the pure perovskite.

Two domains can be distinguished when the TPOIE curves of LM + SiC and LM/YSZ were compared. The trend of the corresponding curves in the "low" temperature domain (below 600 °C) was very similar although they were shifted about 125 °C, which could

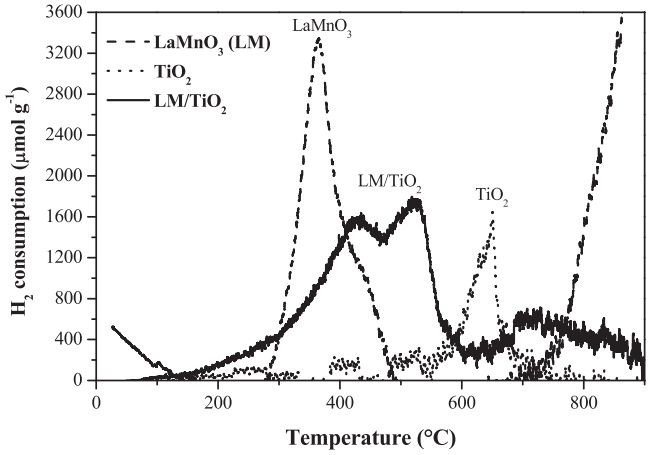

Fig. 10. H_2-TPR profiles of perovskite alone (dash line), TiO_2 alone (dotted line) and LM/TiO_2 (solid line).

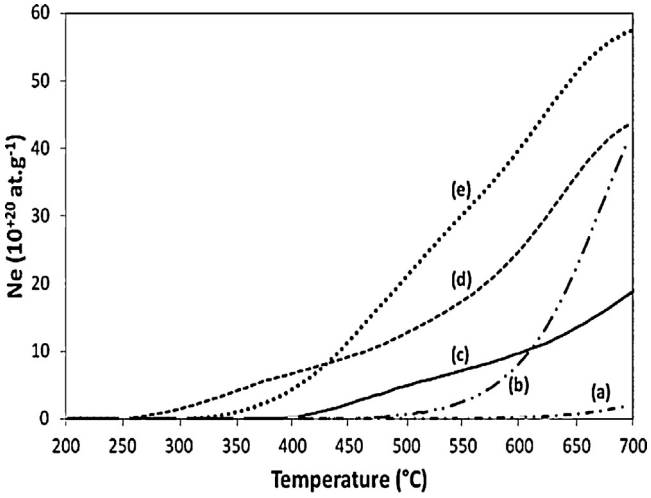

Fig. 11. Evolution of the number of exchanged oxygen atoms (N_e) during the TPOIE experiments on (a) TiO_2, (b) YSZ, (c) LM + SiC, (d) LM/YSZ, and (e) LM/TiO_2.

be attributed to the higher dispersion of $LaMnO_3$ crystallites on YSZ support if compared to those on bulk perovskite. In the "high" temperature domain (above 600 °C), a stronger increase of the N_e value for the supported perovskite was noticed, which was clearly due to a cumulative effect between the oxygen exchanges of $LaMnO_3$ and YSZ matrixes. Regarding LM/TiO_2 catalyst (curve e), a shift of the curve towards lower temperatures (350 °C), if compared with that of the bulk perovskite (curve c), was observed. Nevertheless, the exchange started after that of YSZ-supported $LaMnO_3$ material while the number of atoms exchanged was the most important from 425 °C to 700 °C. Note that this strong increase of the exchange process matched the increase of the $^{16}O_2$ (P_{32}) partial pressure (not shown here); in experiments carried out with pure $LaMnO_3$ this phenomenon took place beyond 550 °C. Such behavior could suggest a synergistic effect between $LaMnO_3$ and TiO_2, leading to an activation of the dioxygen molecule in the form of a diatomic adsorbed species [19]. So, the reaction can take place via a *multiple exchange* ($^{18}O_{2(g)} + 2^{16}O_{(s)} \rightarrow {}^{16}O_{2(g)} + 2^{18}O_{(s)}$), thus leading to the production of $^{16}O_2$ in the gas phase. This specific behavior observed over LM/TiO_2 could explain the decrease of reduction temperature of TiO_2 previously denoted by H_2-TPR experiments over LM/TiO_2 sample (Fig. 10).

The same materials were studied by IOIE experiments at 450 °C during 1 h in order to extract some kinetics parameters from the

Table 4
Results of IOIE experiments.

Materials	P_{32} (mbar) (60 min)	P_{34} (mbar) (60 min)	N_e (10^{+20} at g^{-1}) (15 min)	N_e (10^{+20} at g^{-1}) (60 min)	R_e (10^{+20} at g^{-1} min^{-1})
TiO_2	0	0	0	0	0
YSZ	0	0.6	0.2	0.5	0
$LaMnO_3$+SiC	0	4.3	1	3.5	0.2
LM/YSZ	0	10.8	6.3	8.6	4.6
LM/TiO_2	4.3	16.5	10.8	19.7	1.6

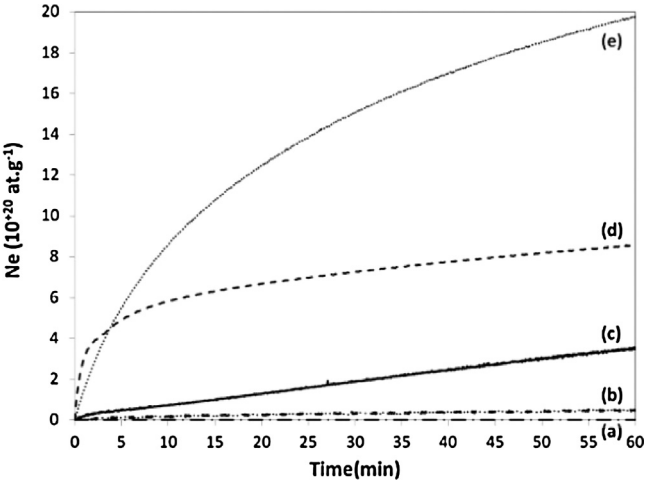

Fig. 12. Evolution of the number of exchanged oxygen atoms (N_e) during the IOIE experiments at 450 °C on (a) TiO_2, (b) YSZ, (c) LM + SiC, (d) LM/YSZ, and (e) LM/TiO_2.

exchanged curves, i.e., the initial rate of exchange (R_e) and the N_e values at 15 and 60 min. Fig. 12 shows the evolution of the number of O atoms exchanged as a function of the time on stream. The results are also listed in Table 4. IOIE curves confirmed the results obtained in TPOIE experiments. Indeed, TiO_2 and YSZ supports did not experience any exchange at 450 °C while in supported $LaMnO_3$ materials an improvement of N_e if compared to that of pure perovskite was observed. The highest number of exchanged O atoms after 60 min was observed for the TiO_2 supported catalyst, being the only one to be detected at a partial pressure of $^{16}O_2$ at 450 °C (Table 4). The *Ne* values normalized per gram of sample and calculated after 60 min were for catalysts LM + SiC, LM/YSZ and LM/TiO_2 $3.5 \times 10^{+20}$, $8.6 \times 10^{+20}$ and $19.7 \times 10^{+20}$ atoms, respectively. The comparison of these values with the total number of O atoms present in $LaMnO_3$ ($15.0 \times 10^{+20}$ at. O) clearly confirmed the hypothesis that O atoms in the TiO_2 support participated in the exchange process via a synergistic effect. On the contrary, it was observed that the exchange in the YSZ support (catalyst LM/YSZ) was not activated at 450 °C. The improvement of N_e on supported materials was accompanied by an increase of the initial rate of exchange especially for catalyst LM/YSZ. This increase was twenty times higher than that observed in pure $LaMnO_3$, thus confirming the higher dispersion of $LaMnO_3$ crystallites when supported on YSZ.

4. Conclusions

The $LaMnO_3$ perovskite phase interacted with TiO_2 and Y_2O_3–ZrO_2 supports in a manner that affected the catalytic activity for toluene oxidation. The catalytic stability was confirmed for all catalysts during three consecutive runs and long-term experiments. The isotopic exchange results matched well the catalytic tests. Indeed, supported materials showed a higher rate of oxygen exchange and a higher catalytic activity for the toluene oxidation than pure perovskite, which could be attributed, in sample LM/YSZ, to the perovskite-support interaction and the oxygen vacancies of the YSZ, whereas in the case of LM/TiO_2 to the activation of the support.

Acknowledgements

The authors gratefully acknowledge China Scholarship Council for the Joint-Training Scholarship Program with Institut de Recherches sur la Catalyse et l'Environnement de Lyon (IRCELYON) and Université Claude Bernard Lyon 1(UCBL1).

Appendix A. Supplementary data

Supplementary data associated with this article can be found, in the online version, at http://dx.doi.org/10.1016/j.apcatb.2015.06.005

References

[1] Regulation (EC) No 715/2007 of the European parliament and of the council of 20 June 2007 on type approval of motor vehicles with respect to emissions from light passenger and commercial vehicles (Euro 5 and Euro 6) and on access to vehicle repair and maintenance information, Official Journal of the European Union, (2007) p. 1–16.
[2] D.B. Meadowcroft, Low-cost oxygen electrode material, Nature 226 (1970) 847–848.
[3] W.B. Li, J.X. Wang, H. Gong, Catalytic combustion of VOCs on non-noble metal catalysts, Catal. Today 148 (2009) 81–87.
[4] P. Ciambelli, V. Palma, S.F. Tikhov, V.A. Sadykov, L.A. Isupova, L. Lisi, Catalytic activity of powder and monolith perovskites in methane combustion, Catal. Today 47 (1999) 199–207.
[5] K.D. Campbell, Layered and double perovskites as methane coupling catalysts, Catal. Today 13 (1992) 245–253.
[6] G. Biausque, Y. Schuurman, The reaction mechanism of the high temperature ammonia oxidation to nitric oxide over $LaCoO_3$, J. Catal. 276 (2010) 306–313.
[7] J. Zhu, A. Thomas, Perovskite-type mixed oxides as catalytic material for NO removal, Appl. Catal. B: Environ. 92 (2009) 225–233.
[8] P.K. Gallagher, D.W. Johnson Jr, J.P. Remeika, F. Schrey, L.E. Trimble, E.M. Vogel, R.J.H. Voorhoeve, The activity of $La_{0.7}Sr_{0.3}MnO_3$ without Pt and $La_{0.7}Pb_{0.3}MnO_3$ with varying Pt contents for the catalytic oxidation of CO, Mater. Res. Bull. 10 (1975) 529–538.
[9] W.P. Stege, L.E. Cadús, B.P. Barbero, $La_{1-x}Ca_xMnO_3$ perovskites as catalysts for total oxidation of volatile organic compounds, Catal. Today 172 (2011) 53–57.
[10] N. Yamazoe, Y. Teraoka, Oxiation catalysis of perovskites-relationships to bulk structure and composition (valency, defect, etc.), Catal. Today 8 (1990) 175–199.
[11] C. Zhang, C. Wang, W. Zhan, Y. Guo, Y. Guo, G. Lu, A. Baylet, A. Giroir-Fendler, Catalytic oxidation of vinyl chloride emission over $LaMnO_3$ and $LaB_{0.2}Mn_{0.8}O_3$ (BCo, Ni, Fe) catalysts, Appl. Catal. B: Environ. 129 (2013) 509–516.
[12] G. Groppi, M. Bellotto, C. Cristiam, P. Forzatti, P.L. Villa, Preparation and characterization of hexaaluminate-based materials for catalytic combustion, Appl. Catal. A: Gen. 104 (1993) 101–108.
[13] R.C. Ropp, G.G. Libowitz, The nature of the alumina-rich phase in the system La_2O_3–Al_2O_3, J. Am. Ceram. Soc. 61 (1978) 473–475.
[14] G. Zou, Z. Wang, M. Sun, X. Luo, X. Wang, A novel solid-gas process to synthesize $LaMnO_3$ perovskite with high surface area and excellent activity for methane combustion, J. Nat. Gas Chem. 20 (2011) 294–298.
[15] R.K.C. de Lima, M.S. Batista, M. Wallau, E.A. Sanches, Y.P. Mascarenhas, E.A. Urquieta-Gonzalez, High specific surface area LaFeCo perovskites-synthesis by nanocasting and catalytic behavior in the reduction of NO with CO, Appl. Catal. B: Environ. 90 (2009) 441–450.
[16] A. González, E. Martínez Tamayo, A. Beltrán Porter, V. Cortés Corberán, Synthesis of high surface area perovskite catalysts by non-conventional routes, Catal. Today 33 (1997) 361–369.

[17] S. Kaliaguine, A. Van Neste, V. Szabo, J.E. Gallot, M. Bassir, R. Muzychuk, Perovskite-type oxides synthesized by reactive grinding: Part I. Preparation and characterization, Appl. Catal. A: Gen. 209 (2001) 345–358.
[18] D. Duprez, In Isotopes in Heterogeneous Catalysis, in: J.S.J. Hargreaves, S.D. Jackson, G. Webb (Eds.), Imperial College Press, London, 2006, p. 133, Chapter 6.
[19] M. Richard, F. Can, D. Duprez, S. Gil, A. Giroir-Fendler, N. Bion, Remarkable enhancement of O_2 activation on yttrium-stabilized zirconia surface in a dual catalyst bed, Angew. Chem. Int. Ed. 53 (2014) 11342–11345.
[20] M. Florea, M. Alifanti, V. Kuncser, D. Macovei, N. Apostol, P. Granger, V.I. Parvulescu, Evidence of A–B site cooperation in the $EuFeO_3$ perovskite from ^{151}Eu and ^{57}Fe Mössbauer spectroscopy, EXAFS, and toluene catalytic oxidation, J. Catal. 316 (2014) 130–140.
[21] J. Zhang, D. Tan, Q. Meng, X. Weng, Z. Wu, Structural modification of $LaCoO_3$ perovskite for oxidation reactions: the synergistic effect of Ca^{2+} and Mg^{2+} co-substitution on phase formation and catalytic performance, Appl. Catal. B: Environ. 172–173 (2015) 18–26.
[22] C.A. Chagas, F.S. Toniolo, R.N.S.H. Magalhães, M. Schmal, Alumina-supported $LaCoO_3$ perovskite for selective CO oxidation (SELOX), Int. J. Hydrogen Energy 37 (2012) 5022–5031.
[23] D. Martin, D. Duprez, Mobility of surface species on oxides. 1. Isotopic exchange of $^{18}O_2$ with ^{16}O of SiO_2, Al_2O_3, ZrO_2, MgO, CeO_2, and CeO_2–Al_2O_3. Activation by noble metals. Correlation with oxide basicity, J. Phys. Chem. 100 (1996) 9429–9438.
[24] S. Ojala, N. Bion, S. Rijo Gomes, R.L. Keiski, D. Duprez, Isotopic oxygen exchange over Pd/Al_2O_3 catalyst: study on $C^{18}O_2$ and $^{18}O_2$ exchange, ChemCatChem 2 (2010) 527–533.
[25] Y. Wang, H. Xu, H. Shang, M. Gong, Y. Chen, Excellent complete conversion activity for methane and CO of Pd/Tio_2-$Zr_{0.5}Al_{0.5}O_{1.75}$ catalyst used in lean-burn natural gas vehicles, J. Energy Chem. 23 (2014) 461–467.
[26] M.A. Fortunato, D. Aubert, C. Capdeillayre, C. Daniel, A. Hadjar, A. Princivalle, C. Guizard, P. Vernoux, Dispersion measurement of platinum supported on yttria-stabilised zirconia by pulse H_2 chemisorption, Appl. Catal. A: Gen. 403 (2011) 18–24.
[27] P.t. M. A. Fortunato, Université Claude Bernard Lyon 1 (France), 2011.
[28] M. Ousmane, L.F. Liotta, G. Pantaleo, A.M. Venezia, G. Di Carlo, M. Aouine, L. Retailleau, A. Giroir-Fendler, Supported Au catalysts for propene total oxidation: study of support morphology and gold particle size effects, Catal. Today 176 (2011) 7–13.
[29] A. Machocki, T. Ioannides, B. Stasinska, W. Gac, G. Avgouropoulos, D. Delimaris, W. Grzegorczyk, S. Pasieczna, Manganese–lanthanum oxides modified with silver for the catalytic combustion of methane, J. Catal. 227 (2004) 282–296.
[30] Y. Lu, Q. Dai, X. Wang, Catalytic combustion of chlorobenzene on modified $LaMnO_3$ catalysts, Catal. Commun. 54 (2014) 114–117.
[31] S. Watanabe, X. Ma, C. Song, Characterization of structural and surface properties of nanocrystalline TiO_2–CeO_2 mixed oxides by XRD, XPS, TPR, and TPD, J. Phys. Chem. C 113 (2009) 14249–14257.
[32] B.C.H. Steele, A. Heinzel, Materials for fuel-cell technologies, Nature 414 (2001) 345–352.